Article

Hydration Structure of Brookite TiO$_2$ (210)

Eero Holmström,*,† Simiam Ghan,† Hitoshi Asakawa,‡ Yasuhiro Fujita,§ Takeshi Fukuma,§,⊥
Sunao Kamimura,# Teruhisa Ohno,⊥,# and Adam S. Foster†,∥

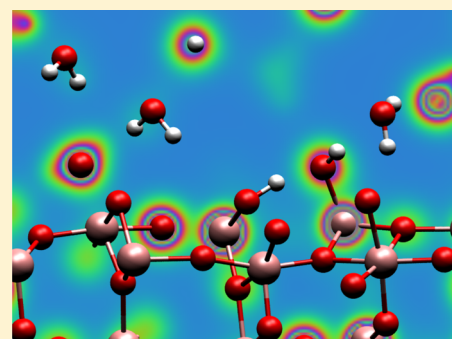†COMP, School of Science, Aalto University, P.O. Box 11100, FI-00076 Aalto, Finland
‡Division of Material Chemistry, §Division of Electrical Engineering and Computer Science, and ∥Frontier Science Organization, Kanazawa University, Kanazawa 920-1192, Japan
⊥Japan Science and Technology Agency, ACT-C, 4-1-8 Honcho, Kawaguchi 332-0012, Japan
#Department of Materials Science, Faculty of Engineering, Kyushu Institute of Technology, Kitakyushu-shi, 804-8550 Fukuoka, Japan

Ⓢ *Supporting Information*

ABSTRACT: The interface of TiO$_2$ and water has been heavily researched due to the photocatalytical capabilities of this system. Whereas the majority of existing work has targeted the rutile and anatase phases of TiO$_2$, much less is known about the brookite phase. In this work, we use first-principles molecular dynamics simulations to find the hydration structure of the brookite (210) surface. We find both pure water and an aqueous solution of KCl to order laterally at the sites of surface Ti cations due to electrostatic and chemical considerations, qualitatively in agreement with experimental high-resolution atomic force microscopy measurements. A significant fraction of surface oxygens is hydroxylated for all cases, with up to 40% realized for the aqueous solution at bulk coverage, a result originating in orientational constraints placed on water near the solvated K and Cl ions. Proton transfer is nearly equally frequent between the surface and liquid regions and within the liquid region, but the presence of K and Cl ions makes proton transfer less efficient.

INTRODUCTION

TiO$_2$ is a photocatalytic metal oxide semiconductor which is used on an industrial scale in such applications as dye-sensitized solar cells, self-cleaning glass, and white pigment.[1−3] The material is also suitable for water-splitting[4,5] and furthermore can be harnessed for water and air purification[1,2] as well as photocatalytic reduction of atmospheric CO$_2$ into hydrocarbons.[6] Under ambient conditions, TiO$_2$ is found in one of the three polymorphs: rutile, anatase, and brookite.[7] While rutile and anatase have received much attention from researchers and are the polymorphs currently applied in the forementioned applications,[1,2,8−10] the brookite phase remains relatively unexplored, partly due to the difficulty of manufacturing this phase of TiO$_2$.[11,12] Subsequently, little is known about the photocatalytical capabilities of brookite for potentially significant applications, in particular the reduction of CO$_2$ into combustible hydrocarbons to close the carbon cycle.[6,13] This reduction reaction is conveniently realized by interfacing TiO$_2$ with a CO$_2$-saturated aqueous solution.[6,13] In addition, it was recently proposed[14] that combining different crystalline phases of TiO$_2$ could improve the efficiency of TiO$_2$ as a photocatalyst for water-splitting.[4,5] For understanding these processes better, the hydration structure of brookite is a property of key importance.

To contribute toward understanding the capability of TiO$_2$ for these promising and environmentally important applications, we use density functional theory (DFT) molecular dynamics (MD) simulations to map the hydration structure of the (210) surface of brookite, which has been predicted from DFT calculations at static conditions[15] to be one of the energetically most favorable cleavages of the crystal. In these static calculations, the (210) cleavage was found to have a surface energy of 0.70 J/m^2, surpassed in stability only by the (001) surface, with the (210) surface covering as much as 33% of the total area of the equilibrium crystal surface, matched only by the (111) cleavage at a coverage of 34%. The adsorption of water onto the (210) surface has been modeled previously under static conditions and at a dilute water coverage, suggesting enhanced chemical activity on this brookite surface with respect to that of the similar TiO$_2$ anatase (101) surface.[16]

In the present work, we use dynamic DFT simulations at varying coverages of water to produce a microscopic model of the ordering of water at this solid−liquid interface, with the ordering being dictated by electrostatic and chemical considerations. We find the surface to be strongly hydroxylated by the indicent liquid, and show that the rates of proton transfer events are lowered by the presence of solvated K and Cl ions. We complement our theoretical calculations with high-resolution atomic force microscopy (AFM) imaging.
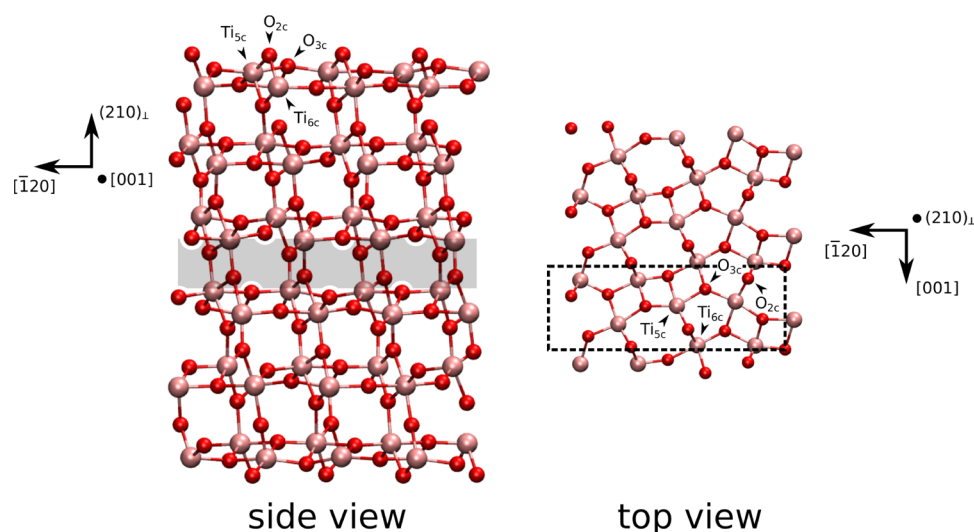
Figure 1. Visualization[23] of the relaxed brookite slab exposing the (210) surface. The shaded area in the side view represents atoms that were fixed during all simulations. The dashed line in the top view indicates the surface unit cell. Atoms are labeled by coordination as described in the text. Ti is pink, and O is red.

COMPUTATIONAL METHODS

To accurately model the solid−liquid interface between brookite and water and hence the hydration structure of the crystal, we performed dispersion-corrected DFT calculations. To describe exchange-correlation effects, we chose the generalized gradient approximation (GGA) level PBE[17] functional augmented by the Grimme D3 dispersion correction,[18] an approach which has recently shown good agreement with experimental results for the $SrTiO_3/H_2O$ interface.[19] A localized basis set of DZVP size[20] and Goedecker−Teter−Hutter pseudopotentials[21] were employed for all elements. The Brillouin zone was sampled only at the Gamma point, an approach justified by the large size of the periodic supercell. All DFT calculations were performed using the CP2K package.[22]

We started by running a static conjugate-gradient geometry optimization of the brookite crystal (of size $2 \times 3 \times 3$ unit cells) in order to obtain the equilibrium lattice constant, bond lengths, bond angles, and the band gap of the material within our DFT-D3 approach. All structural relaxations in this work were run until no total force larger than 0.05 eV/Å was present on any ion in the system. To model the (210) surface of brookite, we constructed a slab of 12 Ti-layers in thickness and 3×1 unit cells of surface area on each of the two slab surfaces, enforcing the equilibrium lattice constant in the lateral direction, and fixing the centermost atomic planes to their bulk equilibrium positions (Figure 1). The rest of the atoms were then allowed to relax through another geometry optimization run. As indicated in Figure 1, the surface comprises 2-fold coordinated bridging oxygen ions ("O_{2c}"), 3-fold coordinated oxygen ions ("O_{3c}"), 5-fold coordinated Ti ions ("Ti_{5c}"), and fully 6-fold coordinated Ti ions ("Ti_{6c}"). The total number of atoms in the slab was 432. A vacuum gap of 20 Å was used between the periodic slab surfaces. Our slab structure is not mirror-symmetric with respect to the central lateral plane, but it is instead mirror-symmetric with a rotation of π radians about the normal vector. Explicit calculations revealed a vanishing vertical dipole for the structure.

To complement our dynamical simulations (see below), we computed static adsorption energies of H_2O onto the brookite surface. To find the ground-state molecular adsorption configuration, we first positioned the intact H_2O molecule over one of several nonequivalent positions on the relaxed (210) surface at a distance of 2 Å and then let the ionic positions relax. To find the dissociative ground-state configuration whereby the water molecule donates one proton to a surface oxygen and an OH fragment is left behind, we took snapshots of dissociated adsorption geometries from our dynamical simulations as initial guesses for the geometry optimization. We used the counterpoise correction[24] to correct for basis set superposition error in these adsorption energies.

To model the full hydration structure, we performed DFT MD simulations within the *NVT* ensemble at $T = 300$ K. The Nosé−Hoover chain thermostat with three links and a time constant of 20 fs, i.e., a frequency of 5×10^{13} Hz, which is in the range of the dominant vibrational frequencies expected in the system (10^{13} Hz for TiO_2 and $2-10 \times 10^{13}$ Hz for H_2O),[25] was used to control the temperature. The time step of the MD simulation was 0.5 fs. We modeled three different coverages of pure water on the surface, 0.5 ML (one monolayer defined here as one H_2O molecule per surface Ti_{5c} cation), 1.0 ML, and a bulk-like coverage, where the total density of water between periodic slab surfaces was constrained to the experimental value of 1 g/cm^3. For the 0.5 and 1.0 ML coverages, the water molecules were initially placed into sheets midway between the crystal surfaces and randomly uniformly rotated about the O ion. For the bulk coverage, the water was initially placed in a regular grid between the slab surfaces, with random rotations applied again to all molecules. The number of H_2O molecules for these three coverages was 12, 24, and 125, respectively. The total duration of each MD run was 20 ps, with ensemble averages being collected over the last 10 ps.

In addition to pure water, we also considered an aqueous solution of KCl on the brookite surface, which is relevant for experimental AFM imaging conditions. By inserting a single pair of K and Cl ions into the simulation cell and removing one H_2O molecule in the process, an effective concentration of 450 mM was realized for the solvated KCl. For these simulations, we used the final configuration of a 15 ps pure-water MD run as the initial configuration of the system. The K and Cl ions were placed on opposing crystal surfaces, and two different starting

positions were considered for each. In addition, we ran one simulation with both ions in the bulk region of the liquid, a few angstroms away from the closest surface.

For all MD runs, we analyzed the vertical density profile of the liquid and the lateral histogram of ionic positions within the observed hydration layers. In addition, we computed the time-dependent O−H coordination of O ions in the supercell, by labeling an O ion at any time step to be coordinated to an H if the latter was within a radius of 1.25 Å of the former. This value of coordination cutoff was justified by the observed O−H radial distribution function of the system. From the time-dependent O−H coordination, we computed the mean fraction of hydroxylated surface oxygens and the rates of proton transfer events at the interface as described in ref 26. Furthermore, we computed the velocity-velocity correlation function of all ions in the liquid region, and Fourier transformed this to find the vibrational density of states[27] for water in the system. Finally, we computed the electronic density of states with projections onto regions of interest. All of these quantities were computed over the final 10 ps of each MD run and averaged where relevant.

EXPERIMENTAL METHODS

Brookite nanorods were prepared by the previously reported procedure.[28] First, 10 g of titanium(IV) ethoxide was added to 50 mL of ethanol solution, and then 3 mL of deionized water was added to the solution. The solution was stirred for 30 min and then centrifugally separated. Amorphous TiO_2 was obtained by drying the specimens in a vacuum oven. Next, 4 g of amorphous titania was dispersed in a water-cooled solution containing 40 mL of 30% H_2O_2 and 10 mL of 28% NH_3. After stirring the mixture for 2 h, 2 g of glycolic acid was added. The color of the mixture changed from yellow to red. After stirring for 24 h to eliminate excess H_2O_2 and NH_3 (aqueous), a titanium glycolated complex solution was obtained. The pH and volume of the complex solution were adjusted to 10 and 50 mL by addition of NH_3 and deionized water. The solution was placed in a sealed Teflon-lined autoclave reactor. The reactor was heated in an oven at 200 °C for 25 h. The substrate was centrifuged, washed with deionized water several times, and dried in a vacuum oven.

The brookite nanorods were fixed on a mica substrate for AFM measurements with an acidic aqueous suspension of 1.0 mg/mL (pH 2.0). The pH of the acidic aqueous suspension was adjusted with dilute hydrochloric acid. The suspension of brookite nanorods (200 μL) was sonicated for 1 min and deposited onto a freshly cleaved mica surface (round disc with a diameter of 12 mm which was purchased from SPI Supplies, West Chester, PA). The sample was incubated for 1 h at room temperature and rinsed with a 100 mM KCl aqueous solution.

We investigated the structures of the brookite nanorods with frequency modulation AFM (FM-AFM). AFM measurements were performed using a custom-built atomic force microscope with an ultralow noise cantilever deflection sensor.[29−31] The microscope was controlled with a commercially available AFM controller (Nanonis RC-4, SPECS Zürich GmbH, Zürich, Switzerland). A silicon cantilever (PPP-NCHAuD, Nanoworld, Headquarters, Switzerland) with a nominal spring constant of 42 N/m and a resonance frequency of 150 kHz in liquid was used. The AFM measurements were performed at room temperature in 100 mM KCl aqueous solution.

RESULTS AND DISCUSSION

In this section, we first present and discuss results from the experimental measurements, then the static DFT calculations, and finally, the DFT MD simulations.

Experiments. We present one large-scale and one magnified FM-AFM image of a brookite nanorod with the (210) facet exposed under 100 mM KCl (aqueous) in Figure 2.
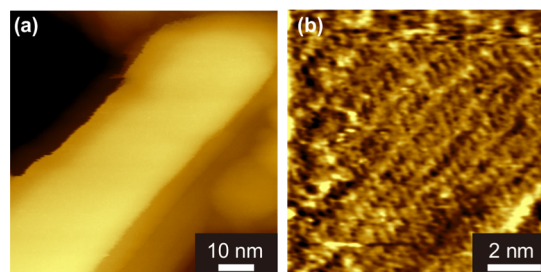

Figure 2. (a) Experimental FM-AFM image of a brookite crystal nanorod exposing the (210) facet under aqueous 100 mM KCl. (b) Close-up of the same.

The close-up image (Figure 2b) which appears to display atomic-scale structure reveals a clearly ordered striped pattern at the solid−liquid interface. While such an ordered pattern in the image might be possibly due to the surface oxygens of the crystal, we assert that it is the first hydration layer of the brookite (210) surface which is being imaged here. We believe this is because the adsorption energy of water on brookite (210) is similar to that on the calcite surface, where it is known that an FM-AFM experiment such as that performed here will result in imaging of the first hydration layer.[32−34] While our present experimental results point to a well-defined hydration structure for brookite (210), a microscopic understanding of the hydration structure requires an atomic-scale model of the structure of the solid−liquid interface. To accomplish this, we turn to DFT simulations for creating a model of the hydration structure.

Static Calculations. *Bulk Brookite Crystal.* We present our results for the bulk brookite crystal in Table 1. In addition to our PBE-D3 results, we also present results obtained using pure PBE for better comparison with previously published DFT calculations.

We predict the lattice parameters of the orthorhombic unit cell of brookite to within ~1% of experimental values, as is typical of GGA-level calculations. Our results are slightly different from previous PBE calculations,[15] which is probably due to differences in choice of basis set and pseudopotential. Our calculations result in a slightly higher spread of Ti−O bond lengths than found in experiment and a much higher spread than in the calculations of Gong and Selloni,[15] which is smaller than that in experiment.[35] The range of O−Ti−O angles that we find is in good agreement with experiment.[35] Finally, our result of 2.3 eV for the band gap of brookite is lower than the experimental value of 3.4 eV.[11] This is to be expected as GGA-level calculations are known to predict band gaps systematically lower than those found in experiment, due to the electronic self-interaction error and the wrongly smooth behavior of the exchange-correlation potential with respect to particle number present in this class of functionals.[36,37]

Brookite (210) Surface in Vacuum. Upon relaxing the slab structure, which was cut out from the optimized bulk crystal, the Ti_{5c} ions move approximately 0.18 Å inward toward the

Table 1. Computed Equilibrium Lattice Parameters (a, b, and c), Ti−O Bond Lengths, O−Ti−O Angles, and Minimum Band Gaps (E_g) for the Bulk Brookite Crystal[a]

method	a (Å)	b (Å)	c (Å)	Ti−O bond lengths (Å)	O−Ti−O angles (deg)	E_g (eV)
PBE, this work	9.28	5.52	5.15	1.85−2.10	76.4−105.4	2.3
PBE-D3, this work	9.25	5.51	5.14	1.85−2.10	76.4−105.5	2.3
PBE[15]	9.14	5.41	5.18	1.93−1.99		
experiment	9.18[35]	5.45[35]	5.15[35]	1.87−2.04[35]	77.0−105.0[35]	3.4[11]

[a]The static computational results are compared to experimental results at 300 K.

center of the slab, whereas the Ti_{6c} and O_{3c} ions move outward by approximately 0.15 and 0.13 Å, respectively. A qualitative explanation for this behavior is that the system seeks to minimize its (free) energy by compensating for the missing Ti−O bonds through pulling the undercoordinated Ti−O_5 polyhedra into the surface where more electronic charge density is available.[15] The bridging O_{2c} ions move no more than 0.01−0.05 Å in the direction normal to the surface upon relaxation.

We find a surface energy of 0.99 J/m^2 for the (210) surface, which is higher than the value of 0.70 J/m^2 found from previous PBE calculations by Gong and Selloni.[15] This discrepancy may again in part be due to differences in the pseudopotentials and basis sets employed, and here also from the inclusion of the D3 correction in our model. We note, however, that from previous hybrid-functional calculations on low-index surfaces of brookite,[38] surface energies consistently 0.2 to 0.4 J/m^2 higher than those reported by Gong and Selloni were found, similar to the difference between our result of 0.99 J/m^2 versus their result of 0.70 J/m^2.[15]

Adsorption of H_2O onto the Brookite (210) Surface. We present the most favorable adsorption geometries of H_2O on brookite in Figure 3. We find molecular adsorption, i.e., the adsorption of H_2O as an intact molecule onto the surface, to be slightly more favorable than dissociative adsorption, where the molecule breaks into an OH group and a proton, the latter of which binds covalently to a surface O_{2c} ion. The adsorption energy of approximately 1 eV found for both cases, and the slightly higher adsorption energy for the molecular mode are in good agreement with previous PBE calculations.[16]

Bader analysis[39−42] (which we choose over other charge-partitioning schemes due to its reliance on a physical observable, the charge density), gives charges of $+0.63e$, $+0.64e$, and $−1.2e$ for H, H, and O, respectively, of water adsorbed in the molecular configuration, the corresponding results for the dissociative case being $+0.62e$, $+0.65e$, and $−1.1e$, where the first charge is for the H bound to the surface O_{2c} anion. Comparing these charges to the case of the isolated H_2O molecule in vacuum, where the charges are $+0.39e$ for H and $−1.2e$ for O, we see that upon adsorption the H_2O molecule donates approximately $0.5e$ of charge to the crystal. We find a significant accumulation of negative charge between the OH fragment and the underlying Ti_{5c} cation in the dissociative configuration and a smaller accumulation of negative charge between the O of the H_2O and the close-lying Ti_{5c} in the molecular adsorption configuration (Figure 3). The former case, in particular, is indicative of a bond of covalent character between the adsorbed OH and the underlying surface cation.

Molecular Dynamics. *Hydration Structure.* We present the hydration structure of pure water on the brookite (210) surface as given by the DFT MD simulations in Figure 4. As results for the two slab surfaces of each DFT MD simulation
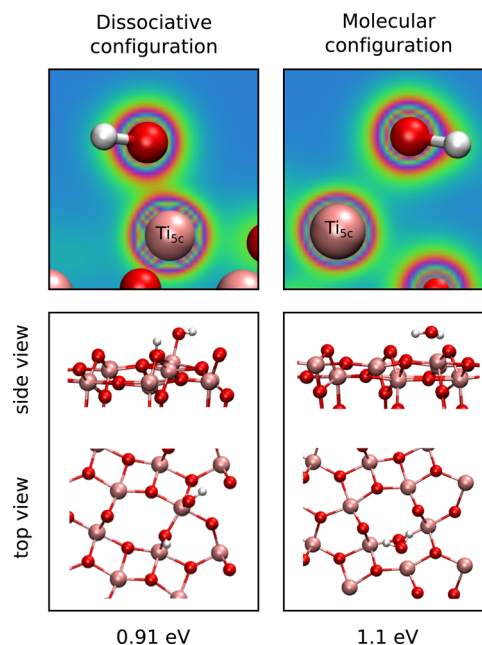

Figure 3. Relaxed dissociative (left) and molecular (right) ground-state adsorption geometries of H_2O on brookite (210) from static geometry relaxations. Top: electronic charge density in a plane through the adsorbed OH fragment and the underlying Ti cation (left), and molecular H_2O and the underlying Ti cation (right). Red indicates high electron density and blue low electron density. Bottom: ball-and-stick model of the adsorption geometries. The corresponding energies of adsorption, including the counterpoise correction to the basis set superposition error, are given. For the atomic models, Ti is pink, O is red, and H is white.

showed no significant differences, for clarity, we present results only for one of the slab surfaces.

For all coverages, the vertical density profile of the hydration structure is dominated by two prominent peaks in the oxygen density, at distances of approximately 2 and 3 Å from the crystal surface, respectively. Overall, the water appears vertically ordered up to midway between the slab surfaces (~8 Å). Hydrogen density found below the lowest-lying oxygen peak is due to surface hydroxylation, i.e., the formation of O_{2c}−H upon dissociative adsorption of water, as well as water molecules donating hydrogen bonds and hence orienting their hydrogens toward surface O_{2c} upon adsorbing in a configuration very similar to that found above from the static calculations of molecular adsorption (Figure 3). Indeed, the brookite (210) surface shows a tendency to dissociate water and to become hydroxylated. In equilibrium, approximately 5, 15, and 20% of surface O_{2c} are covalently bonded to a proton for 0.5 and 1.0 ML and bulk coverages of water, respectively (see below for details). We find all OH fragments within the liquid region stay
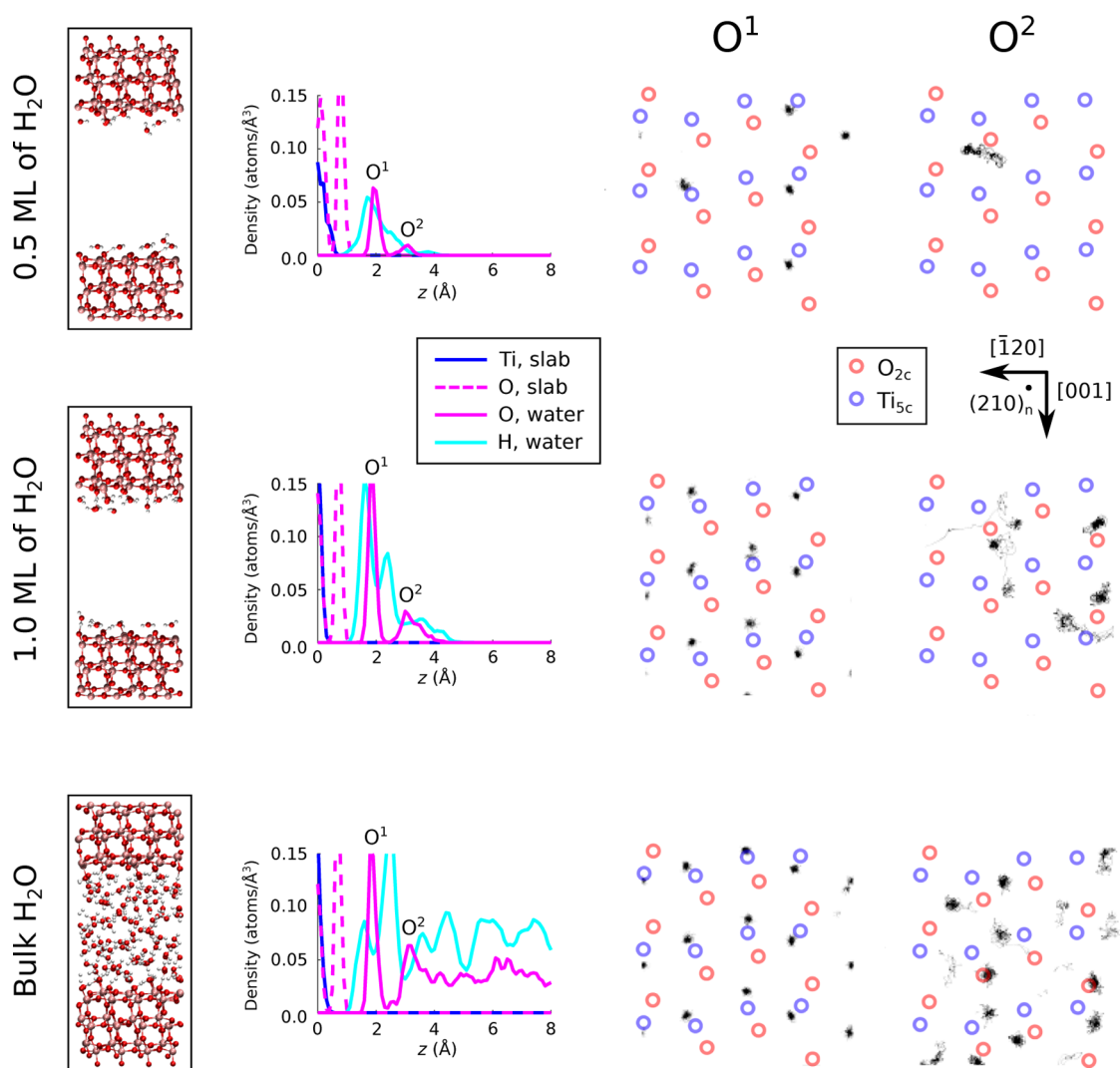
Figure 4. Hydration structure of pure water on brookite (210) from DFT MD, averaged for each coverage over the last 10 ps of a 20 ps run. Results are presented for three coverages: 0.5 ML (top), 1.0 ML (middle), and bulk water (bottom). For each coverage, a snapshot of the equilibrated ionic structure, the vertical density profile, and the histogram of lateral positions of oxygens within the first two oxygen density peaks (O_1 and O_2) are shown. A structural snapshot of the equilibrated trajectory for each of the three DFT MD runs is given in the Supporting Information.

in the first hydration layer, i.e., within the first oxygen peak in the vertical density profile.

The lateral position histograms reveal that oxygens in the first hydration layer assume equilibrium positions slightly off but nearly atop the Ti_{5c} ions in the surface. The ordered pattern of adsorbed water at bulk coverage appears qualitatively consistent with the experimental images presented above (Figure 2). Molecular water is in a configuration close to that found above from the static relaxations (Figure 3), and the oxygens within OH fragments in the liquid region assume lateral positions corresponding to those of the molecularly adsorbed water. In other words, H_2O and OH cannot be distinguished in the hydration structure based solely on their lateral positions. Through inspecting the electronic charge density, we find that these OH and H_2O bind to the underlying surface cations through bonds of partially covalent character as found from our static calculations above (Figure 3). In addition, the electrostatic interaction between the positively charged Ti and the negatively charged O in H_2O and OH adds to the attraction between the surface and the adsorbants. The second

hydration layer displays no obvious lateral ordering of the water.

In Figure 5, we present the hydration structure of the brookite surface under the aqueous 450 mM solution of KCl. For all initial positionings of the K^+ and Cl^- ions, the first peak in the oxygen density profile is nearly identical to the case of pure water. The histograms of lateral oxygen positions show that the horizontal ordering of water in the first hydration layer is also practically the same for KCl 450 mM (aqueous) as that for pure water, except for the fact that the Cl^- ion adsorbed nearly on top of a Ti_{5c} surface cation (cases (a) and (b)) leaves no room for H_2O or OH to adsorb at the expected site in this region. The K^+ ion prefers to adsorb close to surface oxygens, which is to be expected based on simple electrostatics. We find shared electronic charge density between Cl^- and the closest-lying Ti_{5c} ion, indicating an interaction of partial covalent character, whereas the interaction between the K^+ and O_{2c} ions appears purely ionic. In the second hydration layer, no significant difference can be claimed between the oxygen peak in the case of the aqueous solution and pure water, either. For the first case of a surface with an adsorbed K^+ ion (case
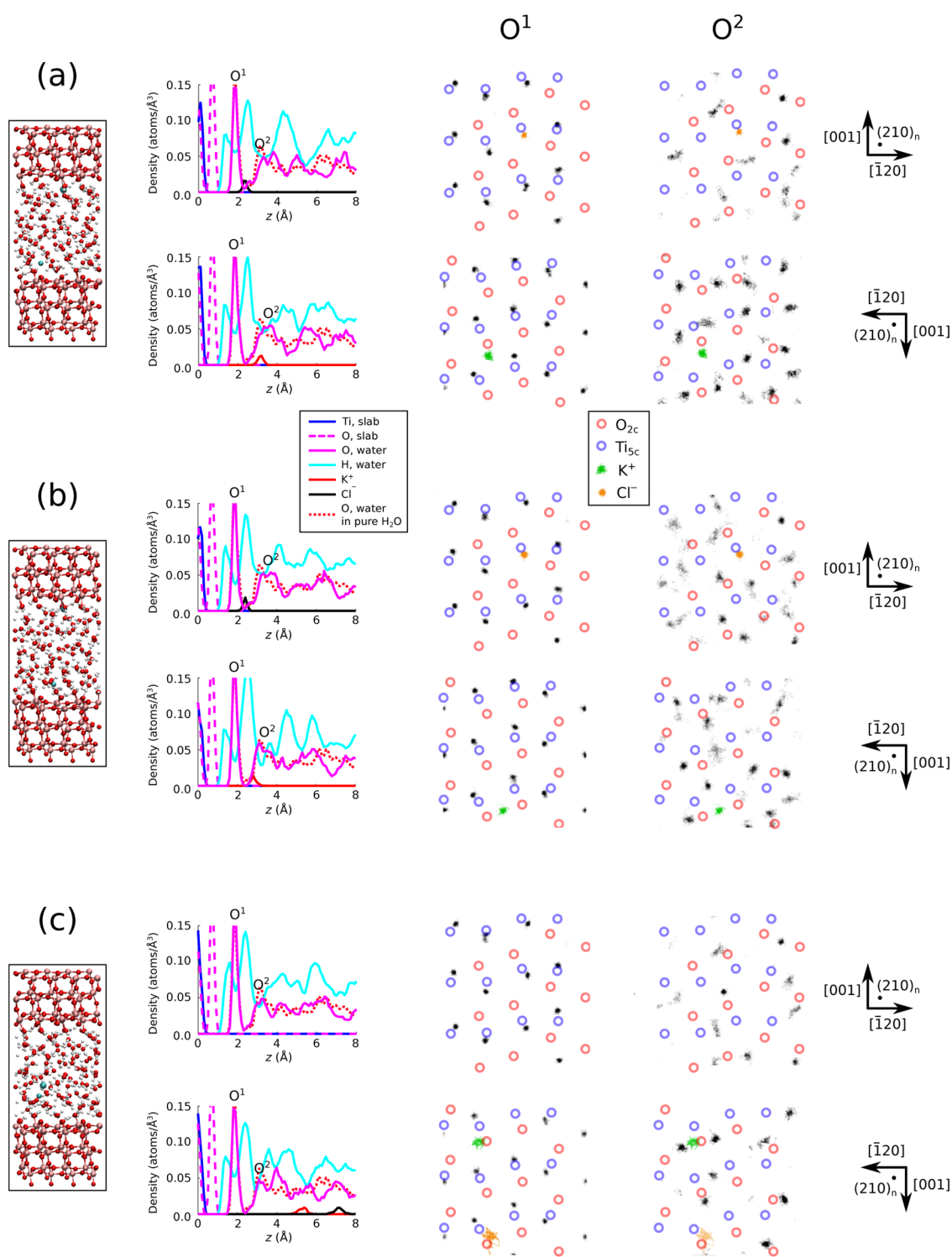
Figure 5. Hydration structure of 450 mM KCl (aqueous) on brookite (210) from DFT MD, averaged for each case over the last 10 ps of a 20 ps run. Results are presented for different initial positions of the K^+ and Cl^- ions: (a) on the surface, (b) another configuration on the surface, and (c) in the bulk region of the liquid. For each case, a snapshot of the equilibrated ionic structure, the vertical density profile, and the histogram of lateral positions of oxygens within the first two oxygen density peaks (O_1 and O_2) are shown. The density profile of O in pure water (from Figure 4) is plotted for comparison. A structural snapshot of the equilibrated trajectory for each of the three DFT MD runs is given in the Supporting Information.

(a)), there is some hint of lateral ordering of the second hydration layer, but no ordering can be claimed for the other cases ((b) and (c)).

For quantifying the hydration of the solvated K^+ and Cl^- ions in bulk water (system (c) above), we computed the K–O, K–

H, Cl–O, and Cl–H radial distribution functions (RDF) (Figure 6). For K^+, we find the first oxygen peak to lie at approximately $r = 2.8$ Å with the first hydrogen peak further out at $r = 3.5$ Å, signaling that the positively charged K^+ ion binds favorably to the negatively charged O ions of the H_2O and OH
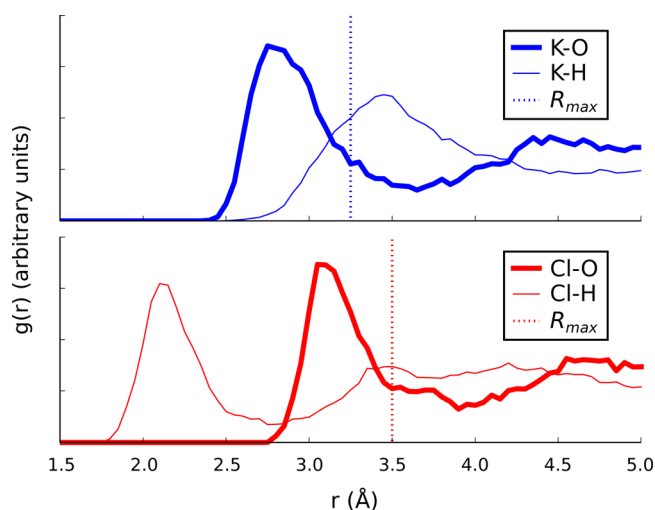
Figure 6. Partial radial distribution functions for K−O, K−H, Cl−O, and Cl−H for the system with KCl dissolved into the bulk region of the liquid away from the surface (case c), averaged over the last 10 ps of a 20 ps DFT MD run. Integration limits for determining the nearest-neighbor water coordination numbers are shown as dashed vertical lines.

molecules and that the H_2O and OH are oriented so that the oxygens are closest to the K^+ ion and the hydrogens are pointed outward from the shell of oxygens. The reverse situation is found for the negatively charged Cl^- ion, with the first hydrogen peak at $r = 2.1$ Å and the first oxygen peak at $r = 3.1$ Å, reflecting that the H_2O and OH donate hydrogen bonds to the Cl^- ion and that the orientation of the binding molecules is reversed from the case of K^+. We find the K−O and Cl−O coordination numbers by integrating the relevant RDF up to the first minimum after the first peak (R_{max}):

$$\langle Z \rangle = \rho_0 \int_0^{R_{max}} g(r)\, 4\pi r^2\, \mathrm{d}r \qquad (1)$$

with a result of ∼6 for both $\langle Z \rangle_{K-O}$ and $\langle Z \rangle_{Cl-O}$. These results are in excellent agreement with the emerging consensus of a value of $\langle Z \rangle_{K-O} \approx 6$ from experimental and computational work[43] and the value of $\langle Z \rangle_{Cl-O} \approx 6.4 \pm 0.3$ from experiment.[44] For the Cl^- ion, Bader analysis gives an average charge of $(-0.594 \pm 0.005)e$, $(-0.608 \pm 0.004)e$, and $(-0.708 \pm 0.003)e$ in systems (a)−(c), respectively. The corresponding results for K^+ are $(0.887 \pm 0.001)e$, $(0.889 \pm 0.001)e$, and $(0.898 \pm 0.001)e$. Finally, we compute the mean total energies E of systems (a)−(c) to find that the energy of the system is slightly lower when KCl is dissolved into the bulk region of the liquid as compared to that when K^+ and Cl^- are adsorbed onto the surface ($E_a = 0.00 \pm 0.15$ eV, $E_b = -0.46 \pm 0.11$ eV, and $E_c = -0.63 \pm 0.08$ eV). Here E_b and E_c are within error bounds of each other, but the higher configurational entropy of the state where KCl is dissolved into the bulk liquid would likely make the free energy difference significant between the two. It therefore appears that adsorption of K^+ and Cl^- ions onto the brookite surface is not thermodynamically favorable under these conditions. This finding appears in contrast to earlier work on the rutile (110) surface, where experiments suggested the formation of KCl precipitates originating from the aqueous KCl interfaced with the TiO_2 surface.[45] The concentration of the KCl solution in this previous study was, however,

approximately twice as high as that in the present work (1 M vs 450 mM, respectively).

Interestingly, the hydroxylation fraction of the brookite (210) surface is considerably higher for the case of the KCl (aqueous)eous solution than for pure water (Figure 7). The
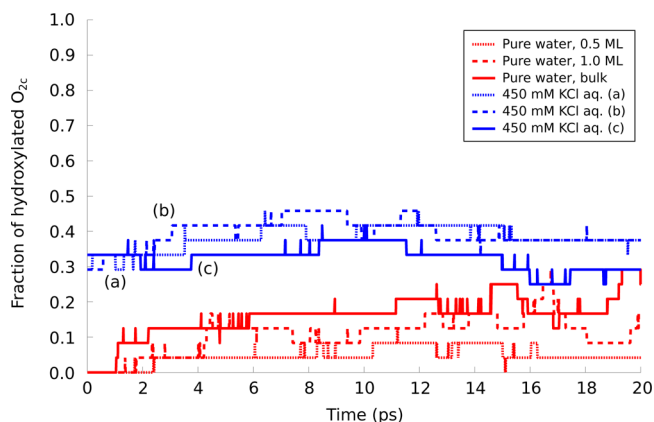

Figure 7. Degree of surface hydroxylation vs time, i.e., the time evolution of the fraction of bridging surface oxygens (O_{2c}) hydroxylated into O_{2c}−H in the DFT MD simulations, showing the initial 10 ps equilibration period and the subsequent 10 ps over which averages for the hydroxylation fraction were computed. Results for the systems with KCl (aqueous) are presented for different initial positions of the K^+ and Cl^- ions: (a) on the surface, (b) another configuration on the surface, and (c) in the bulk region of the liquid.

situation where the K^+ and Cl^- ions are solvated into the bulk liquid away from the surface gives the lowest degree of hydroxylation of the three KCl-containing simulations, but even this level is higher than that for pure water (∼30% vs ∼20%). The cases where the K^+ and Cl^- ions are adsorbed onto the surface ((a) and (b)) display mean hydroxylation fractions as high as 40%. While fluctuations in the hydroxylation fraction as a function of time are large (up to ∼10%), the difference of some 20% in the quantity between the cases of pure water and the aqueous solution of KCl is significant.

To explain this, we propose the following. For the free energy of dissociation $\Delta F_{diss} = \Delta E_{diss} - T\Delta S_{diss}$, we take $\Delta E_{diss} > 0$ from our static calculations (and assume that solvating the molecularly or dissociatively adsorbed water molecule would leave the sign for this quantity unchanged), which implies $\Delta S_{diss} > 0$, as otherwise no dissociation is possible. We further assume that ΔE_{diss} is constant, regardless of the composition of the liquid. We then make the approximation that dissociating a single molecule of water adds N microstates to the system, which, taking the entropy of the system to be approximated by $S = k_B \log \Omega$ implies $\Delta S_{diss} = k_B \log(1 + N/\Omega)$, where Ω is the number of microstates before the dissociation event. We now see that ΔS_{diss} decreases as the surface becomes increasingly hydroxylated. ΔF_{diss} must vanish at the equilibrium hydroxylation fraction f_0 of the equilibrated system of pure water and the brookite crystal, i.e., $\Delta E_{diss} = T\Delta S_{diss}$ in equilibrium. Crucially, when K^+ and Cl^- are added to the system, these ions cause the water molecules in their immediate vicinity to orient themselves as described above. This constrains the range of configurations that the water molecules may assume with any reasonable probability, decreasing Ω and therefore increasing ΔS_{diss}, making the dissociation reaction favorable again. Subsequently, the system proceeds to increase the degree of surface hydroxylation until ΔF_{diss} vanishes again and a new
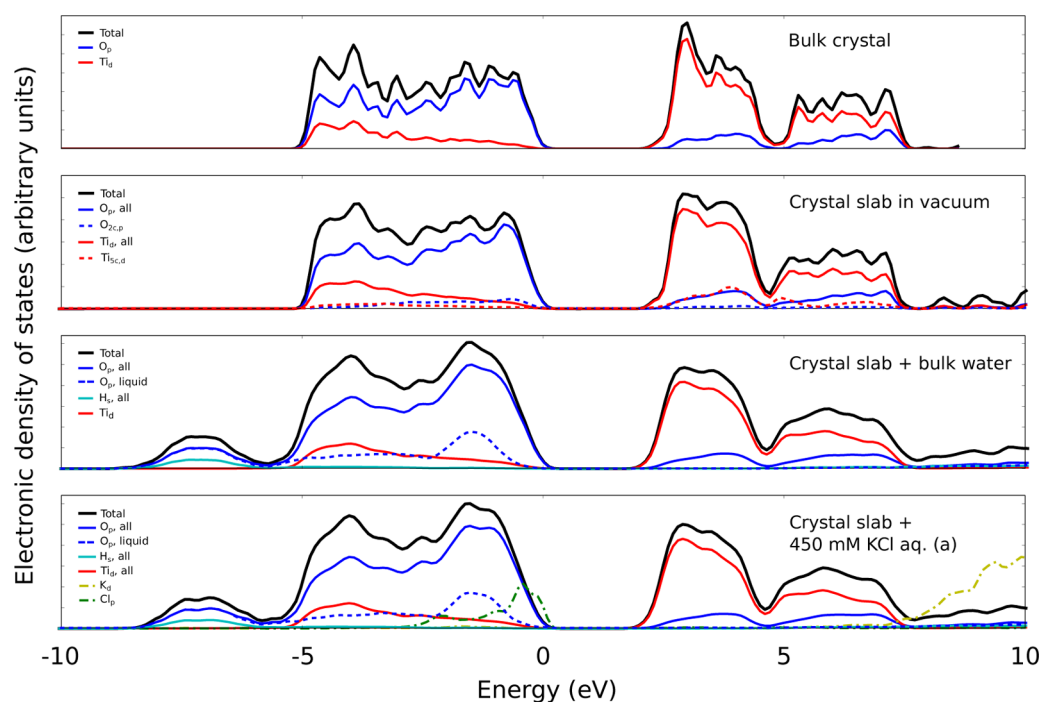
Figure 8. Total and projected electronic density of states (DOS) for various simulated systems. Results for systems involving water or KCl (aqueous) are averaged over five snapshots from the DFT MD. The KCl system is one with ions adsorbed onto the slab surface (case a). Projections of the DOS onto the adsorbed K^+ and Cl^- ions have been magnified for clarity. The energy scale has been shifted for all systems individually so that the Fermi energy is at 0 eV.

equilibrium fraction of hydroxylation $f_0' > f_0$ is reached. This picture is consistent with the following observations: (i) No systematic difference is observed in the degree of hydroxylation on the two slab surfaces with the two different ion species incident. (ii) Water in the hydration shell of the Cl^- ion is not dissociated at all. (iii) Surface oxygen charges remain unaltered in the presence of the ions. (iv) The positions of OH groups are not correlated with positions of the adsorbed ions, all of which together seem to rule out a direct chemical effect as the explanation for the increase in the degree of hydroxylation.

Electronic Structure. The electronic density of states (DOS) of the bulk brookite crystal, the crystal slab in vacuum, the slab under a bulk coverage of water, and the slab under the KCl (aqueous) solution with K^+ and Cl^- ions adsorbed onto the surface (case (a) above) is presented in Figure 8. The valence band of the bulk crystal is dominated by p-type orbitals of O, whereas the conduction band is dominated by d-type orbitals of Ti. The same holds true also for the other three systems presented here. The band gap of the crystal is not significantly affected by opening up a free surface or covering the surface with liquid. For the crystal slab in vacuum, contributions from the surface layers (O_{2c} and Ti_{5c}) are well within the valence and conduction bands, respectively, and present no features of particular interest in the DOS.

When the surface is covered with water or the aqueous solution of KCl, we find that a new band of some 3 eV width is formed below the valence band of the clean crystal slab. This band is attributable to the O−H bonds of H_2O and OH in the liquid region of the system, as revealed by the shown projections of the DOS onto O and H within the liquid. Both the K^+ and Cl^- ions have a nominally full 3p shell, and this highest-lying valence subshell of the Cl^- ion is found at the top of the valence band of the brookite and KCl system, with the empty Cl^- 3d shell spread into a band some 15 to 25 eV

beyond the Fermi level (not shown here). The corresponding 3p shell of K^+ lies approximately 11 eV below the Fermi level (not shown here), and the empty 3d shell of K^+ is found at the top of the conduction band some 10 eV beyond the Fermi level.

Vibrational Spectrum. The vibrational densities of states of water and the aqueous solution of KCl at the studied solid−liquid interface are presented in Figure 9. Three major features are visible in all spectra: the low-frequency band corresponding to librational motion of H_2O and OH (centered at ∼600 cm^{-1}), the scissor bending mode of H_2O (centered at ∼1600 to 1700
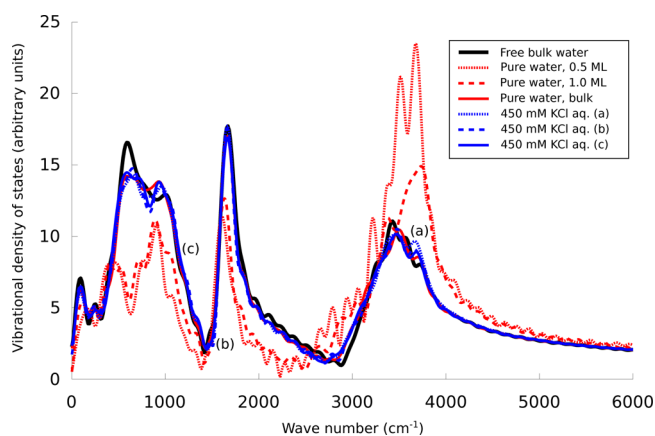

Figure 9. Vibrational spectrum of water, computed after an initial 10 ps equilibration period for each system. For the aqueous solution of KCl, results are presented for different initial positions of the K^+ and Cl^- ions: (a) on the surface, (b) another configuration on the surface, and (c) in the bulk region of the liquid. The vibrational spectrum of a periodic supercell of water with no crystal involved ("Free bulk water") is given for reference.

Table 2. Mean Rate of Proton Transfer Events in All Simulated Systems[a]

	jumps/ps/1 × 1			jumps/ps/OH		
system	surface O	liquid O	total	surface O	liquid O	total
pure water, 0.5 ML	0.40	1.1	1.5	1.7	4.6	6.3
pure water, 1.0 ML	0.52	0.82	1.3	0.94	1.5	2.4
pure water, bulk	0.87	1.9	2.7	1.1	2.4	3.5
450 mM KCl (aqueous) (a)	0.38	1.7	2.1	0.24	1.1	1.3
450 mM KCl (aqueous) (b)	0.20	1.4	1.6	0.13	0.88	1.0
450 mM KCl (aqueous) (c)	0.47	0.97	1.4	0.37	0.78	1.2

[a]In units of "jumps per ps per (1 × 1) surface unit cell" and "jumps per ps per OH fragment". Proton transfer events involving changes in O−H coordination of O in the liquid region and within the crystal surface are separated. Results for systems involving KCl (aqueous) are presented for different initial positions of the K⁺ and Cl⁻ ions: (a) on the surface, (b) another configuration on the surface, and (c) in the bulk region of the liquid.

Table 3. Mean Rate of Proton Transfer Events in All Simulated Systems[a]

	jumps/ps/1 × 1			jumps/ps/OH		
system	surface−liquid	liquid−liquid	total	surface−liquid	liquid−liquid	total
pure water, 0.5 ML	0.40	0.35	0.75	1.7	1.4	3.1
pure water, 1.0 ML	0.52	0.15	0.68	0.94	0.28	1.2
pure water, bulk	0.87	0.51	1.4	1.1	0.65	1.8
450 mM KCl (aqueous) (a)	0.38	0.66	1.0	0.24	0.43	0.67
450 mM KCl (aqueous) (b)	0.20	0.60	0.80	0.13	0.38	0.51
450 mM KCl (aqueous) (c)	0.47	0.25	0.72	0.37	0.21	0.58

[a]Separated into jump events between the surface and liquid regions ("surface−liquid") and jump events within the liquid region ("liquid−liquid"). Rates are given in units of "jumps per ps per (1 × 1) surface unit cell" and "jumps per ps per OH fragment". Results for systems involving KCl (aqueous) are presented for different initial positions of the K⁺ and Cl⁻ ions: (a) on the surface, (b) another configuration on the surface, and (c) in the bulk region of the liquid.

cm^{-1}), and the high-frequency band corresponding to stretching vibrations of the covalent O−H bond (centered at ∼3500 to 3900 cm^{-1}). The vibrational spectra of systems with a bulk coverage of liquid (both pure water and the aqueous solution of KCl) show very little departure from the spectrum of free, pure bulk water. Still, some redshifting or broadening of the O−H stretching band toward lower frequencies is observed for all surfaces at all levels of water coverage. As is known from previous work on TiO$_2$, the cause for this effect is the weakening of covalent O−H bonds in the liquid region due to the molecules bonding with the crystal surface.[46,47] The stronger the water-to-surface bonding, the weaker the covalent O−H bonding within H$_2$O and OH, and hence the lower the O−H stretching band frequencies.

Clear differences from the behavior of free bulk water are observed for the vibrational spectra of the low-coverage (0.5 and 1.0 ML) cases of pure water. For both of these cases, we find the weight of the spectrum to be shifted away from the two lower-frequency bands and into the high-frequency band of O−H stretching vibrations with respect to free bulk water. Reduction in the number of modes in the librational band is to be expected, as with vacuum available between the crystal surfaces, the water has more configurational freedom in space and is not as easily confined to perform librational motion as in the case of bulk coverage of water. To the extent that water in the low-coverage systems can be considered to behave more in a gas-like way than water in the bulk coverage systems, the observation that the bending band is slightly subdued and shifted downward in frequency is in agreement with the experimental result that the bending mode of H$_2$O has a lower frequency in the gas phase than in the liquid phase.[25] Indeed, at low coverages, the water is always in contact with vacuum or free space between the crystal surfaces. This provides the molecules with free space into which the stretching vibrations

can easily be directed. Such little-hindered vibrations of the O−H bond are expected to be of a higher frequency than vibrations into or in the vicinity of other ions, an effect which is seen in the O−H stretching band for the low-coverage systems. An analysis of velocity−velocity correlation functions of individual H ions reveals that this blueshifting is due to the high-frequency stretching modes of both H$_2$O and OH molecules in the liquid. The observation of blueshifting is also in agreement with experimental results showing that the O−H stretching frequency is higher in the gas phase than in the liquid phase of water.[25] When total water coverage is increased from 0.5 to 1.0 ML, the only significant change in the vibrational spectrum is the decrease in the total number of modes in the O−H vibrational band, which happens as the O−H bonds of water molecules are presented, on average, with less free space for performing these high-frequency stretching vibrations.

Proton Dynamics. We present average rates of proton transfer reactions in Table 2, resulting from the O−H coordination analysis described above. In dynamical equilibrium, we observe three kinds of proton transfer events taking place in the simulations. First, we observe surface oxygens donating protons to OH fragments in the liquid. Second, we see the reverse reaction of H$_2$O in the liquid donating protons to the surface. Third, we see proton transfer between H$_2$O and OH within the liquid region. Notably, we see no transfer of protons taking place directly between the surface oxygens.

By examining Table 2, we see that for all simulated systems, proton jumps involving oxygens in the liquid region dominate those involving oxygens of the crystal surface. However, as there is no transfer of protons between surface oxygens, each event involving a surface oxygen corresponds to an event involving a liquid oxygen, as a proton is transferred either way between the liquid and surface regions, and such events are

"double-counted" in the jump rates of Table 2. In addition, each liquid−liquid proton transfer event is double-counted as two events involving liquid oxygens, although only one act of proton transfer takes place. Taking these considerations into account, we separate the jump rates into the categories of surface−liquid jumps and liquid−liquid jumps in Table 3. We now see that for pure water, surface−liquid proton transfer reactions are more frequent than liquid−liquid transfer reactions. For the aqueous solution of KCl, the trend is mixed.

Still, for both compositions of the liquid, the differences between these two categories of jump rates are relatively small, i.e., surface−liquid and liquid−liquid proton transfer rates are similar for any given system. The two rates are generally similar between different systems as well, with the notable exception that OH fragments formed from pure water seem much more efficient in facilitating surface−liquid proton jumps than OH fragments formed within systems containing the aqueous KCl solution do. Two reasons can be found for this observation. First, because of their large size, the K^+ and Cl^- ions hinder proton transfer with their presence in the system. This is supported by the fact that as the ions are moved from the surface into the bulk liquid (systems (a) and (b) vs (c)), surface−liquid jump rates go up, and liquid−liquid jump rates go down. The second reason for the average OH fragment being more efficient in causing surface−liquid proton transfer in pure water is simply that there are less OH fragments in pure water (Figure 7), which means that on average each OH fragment is surrounded by less competitors attempting to grab protons from nearby surface sites. Finally, jump rates per formed OH fragment are clearly higher for the lowest coverage of water than in other systems. This result probably reflects the large availability of high-frequency O−H stretching modes found for water in this system (Figure 9), vibrational modes which are expected to facilitate the transfer of protons within the system.

Implications of Our Results for Other TiO$_2$ Surfaces and the Photocatalytic Activity of Brookite. The structure of the brookite (210) surface can be characterized by rectangular building blocks arranged in varying lateral orientations along different ⟨001⟩ rows on the surface.[15] Whereas the commonly encountered rutile (110) surface similarly consists of undercoordinated (4-fold-coordinated) Ti cations and 2-fold coordinated bridging oxygens,[46] quantitative differences in the atomic arrangements between these two surfaces are significant. However, as pointed out by Gong and Selloni,[15] the brookite (210) surface may be considered a distorted version of the anatase (101) surface, where the rectangular building blocks of the surface structure all have the same orientation. It is therefore reasonable to assume that our results for the hydration structure of brookite (210) are transferable to some degree to anatase (101), regarding in particular the lateral and vertical ordering of oxygen in the liquid region with respect to the crystal surface. However, statically computed[16] adsorption energies of water in the molecular and dissociated states on anatase (101) (0.71 vs 0.38 eV, respectively) as compared to brookite (210) (1.02 vs 0.97 eV, respectively) would imply that the degree of hydroxylation on the anatase surface is much lower than that on brookite.

Interestingly, it was recently discovered that hydroxylation of the anatase TiO$_2$ surface leads to enhanced photocatalytic efficiency for hydrogen production.[48,49] We find a high degree of surface hydroxylation (up to 40%) on the studied brookite (210) surface. It is reasonable to suggest that the predicted strong hydroxylation of the brookite surface will lead to enhanced photocatalytic activity for this material as well, possibly even beyond that of anatase, as has been reported for several applications.[12]

■ CONCLUSIONS

Using dispersion-corrected density functional theory molecular dynamics simulations, we present a model for the hydration structure of the (210) surface of the brookite phase of TiO$_2$. We find water at the solid−liquid interface to order laterally in registry with the crystal surface due to strong, partially covalent bonding with underlying Ti surface cations, in qualitative agreement with high-resolution atomic force microscopy measurements. Up to 40% of surface oxygens are hydroxylated at bulk coverages of the incident liquid, with higher hydroxylation fractions found for the case of aqueous solutions of KCl than for pure water, an effect that we propose is due to entropic considerations. The presence of solvated K and Cl ions reduces the efficiency of proton transfer reactions at the interface region. The predicted degree of hydroxylation of the brookite surface as well as the computed rates of proton transfer are likely to be useful in future studies of the suitability of this solid−liquid interface for photocatalytical applications. Further experimental work is necessary in order to validate the first-principles results presented here for the hydration structure of the brookite crystal.

■ ASSOCIATED CONTENT

ⓢ Supporting Information
The Supporting Information is available free of charge on the ACS Publications website at DOI: 10.1021/acs.jpcc.7b05524.

Snapshots of the equilibrated trajectory of the DFT MD runs for the brookite/water interface at the three studied coverages of 0.5 ML, 1.0 ML, and bulk water (pure_water_brookite_0.5_ML.xyz, pure_water_brookite_1.0_ML.xyz, and pure_water_brookite_bulk_coverage.xyz, respectively) and for the brookite/KCl (aqueous) interface for the three studied cases a, b, and c as denoted in the main article (brookite_KCl_aq_a.xyz, brookite_KCl_aq_b.xyz, and brookite_KCl_aq_c.xyz, respectively) (ZIP)

■ AUTHOR INFORMATION

Corresponding Author
*E-mail: eero.holmstrom@aalto.fi.
ORCID ⓞ
Eero Holmström: 0000-0002-4866-3730
Takeshi Fukuma: 0000-0001-8971-6002
Adam S. Foster: 0000-0001-5371-5905
Notes
The authors declare no competing financial interest.

■ ACKNOWLEDGMENTS

■ REFERENCES

(1) Diebold, U. The Surface Science of Titanium Dioxide. *Surf. Sci. Rep.* **2003**, *48*, 53−229.

(2) Gupta, S. M.; Tripathi, M. A Review of TiO₂ Nanoparticles. *Chin. Sci. Bull.* **2011**, *56*, 1639−1657.

(3) Wang, Y.; Li, J.; Wang, L.; Xue, T.; Qi, T. Preparation of Rutile Titanium Dioxide White Pigment via Doping and Calcination of Metatitanic Acid Obtained by the NaOH Molten Salt Method. *Ind. Eng. Chem. Res.* **2010**, *49*, 7693−7696.

(4) Fujishima, A.; Honda, K. Electrochemical Photolysis of Water at a Semiconductor Electrode. *Nature* **1972**, *238*, 37−38.

(5) Catlow, C. R. A.; Guo, Z. X.; Miskufova, M.; Shevlin, S. A.; Smith, A. G. H.; Sokol, A. A.; Walsh, A.; Wilson, D. J.; Woodley, S. M. Advances in Computational Studies of Energy Materials. *Philos. Trans. R. Soc., A* **2010**, *368*, 3379−3456.

(6) Inoue, T.; Fujishima, A.; Konishi, S.; Honda, K. Photo-electrocatalytic Reduction of Carbon Dioxide in Aqueous Suspensions of Semiconductor Powders. *Nature* **1979**, *277*, 637−638.

(7) Zhu, T.; Gao, S.-P. The Stability, Electronic Structure, and Optical Property of TiO₂ Polymorphs. *J. Phys. Chem. C* **2014**, *118*, 11385−11396.

(8) Diebold, U. Structure and Properties of TiO₂ Surfaces: a Brief Review. *Appl. Phys. A: Mater. Sci. Process.* **2003**, *76*, 681−687.

(9) Ni, M.; Leung, M. K. H.; Leung, D. Y. C.; Sumathy, K. A Review and Recent Developments in Photocatalytic Water-Splitting using TiO₂ for Hydrogen Production. *Renewable Sustainable Energy Rev.* **2007**, *11*, 401−425.

(10) Daghrir, R.; Drogui, P.; Robert, D. Modified TiO₂ for Environmental Photocatalytic Applications: a Review. *Ind. Eng. Chem. Res.* **2013**, *52*, 3581−3599.

(11) Hu, W.; Li, L.; Li, G.; Tang, C.; Sun, L. High-Quality Brookite TiO₂ Flowers: Synthesis, Characterization, and Dielectric Performance. *Cryst. Growth Des.* **2009**, *9*, 3676−3682.

(12) Di Paola, A.; Bellardita, M.; Palmisano, L. Brookite, the Least Known TiO₂ Photocatalyst. *Catalysts* **2013**, *3*, 36−73.

(13) Habisreutinger, S. N.; Schmidt-Mende, L.; Stolarczyk, J. K. Photocatalytic Reduction of CO₂ on TiO₂ and Other Semiconductors. *Angew. Chem., Int. Ed.* **2013**, *52*, 7372−7408.

(14) Buckeridge, J.; Butler, K. T.; Catlow, C. R. A.; Logsdail, A. J.; Scanlon, D. O.; Shevlin, S. A.; Woodley, S. M.; Sokol, A. A.; Walsh, A. Polymorph Engineering of TiO2: Demonstrating How Absolute Reference Potentials Are Determined by Local Coordination. *Chem. Mater.* **2015**, *27*, 3844−3851.

(15) Gong, X.-Q.; Selloni, A. First-Principles Study of the Structures and Energetics of Stoichiometric Brookite TiO₂ Surfaces. *Phys. Rev. B: Condens. Matter Mater. Phys.* **2007**, *76*, 235307.

(16) Li, W.-K.; Gong, X.-Q.; Lu, G.; Selloni, A. Different Reactivities of TiO₂ Polymorphs: Comparative DFT Calculations of Water and Formic Acid Adsorption at Anatase and Brookite TiO₂ Surfaces. *J. Phys. Chem. C* **2008**, *112*, 6594−6596.

(17) Perdew, J. P.; Burke, K.; Ernzerhof, M. Generalized Gradient Approximation Made Simple. *Phys. Rev. Lett.* **1996**, *77*, 3865.

(18) Grimme, S.; Antony, J.; Ehrlich, S.; Krieg, H. A Consistent and Accurate Ab Initio Parametrization of Density Functional Dispersion Correction (DFT-D) for the 94 Elements H-Pu. *J. Chem. Phys.* **2010**, *132*, 154104.

(19) Kawasaki, S.; Holmström, E.; Takahashi, R.; Spijker, P.; Foster, A. S.; Onishi, H.; Lippmaa, M. Intrinsic Superhydrophilicity of Ti-Oxide Surfaces. *J. Phys. Chem. C* **2017**, *121*, 2268−2275.

(20) VandeVondele, J.; Hutter, J. Gaussian Basis Sets for Accurate Calculations on Molecular Systems in Gas and Condensed Phases. *J. Chem. Phys.* **2007**, *127*, 114105.

(21) Hartwigsen, C.; Goedecker, S.; Hutter, J. Relativistic Separable Dual-Space Gaussian Pseudopotentials from H to Rn. *Phys. Rev. B: Condens. Matter Mater. Phys.* **1998**, *58*, 3641−3662.

(22) Hutter, J.; Iannuzzi, M.; Schiffmann, F.; VandeVondele, J. CP2K: Atomistic Simulations of Condensed Matter Systems. *Wiley Interdiscip. Rev.: Comput. Mol. Sci.* **2014**, *4*, 15−25.

(23) Humphrey, W.; Dalke, A.; Schulten, K. VMD - Visual Molecular Dynamics. *J. Mol. Graphics* **1996**, *14*, 33−38.

(24) Leach, A. R. *Molecular Modelling: Principles and Applications*, 2nd ed.; Pearson Education: Harlow, U.K., 2001.

(25) Chen, S.-H.; Toukan, K.; Loong, C.-K.; Price, D. L.; Teixeira, J. Hydrogen-Bond Spectroscopy of Water by Neutron Scattering. *Phys. Rev. Lett.* **1984**, *53*, 1360−1363.

(26) Holmström, E.; Spijker, P.; Foster, A. S. The Interface of SrTiO₃ and H₂O from First-Principles Molecular Dynamics. *Proc. R. Soc. London, Ser. A* **2016**, *472*, 20160293.

(27) Dickey, J. M.; Paskin, A. Computer Simulation of the Lattice Dynamics of Solids. *Phys. Rev.* **1969**, *188*, 1407−1418.

(28) Zhang, L.; Menendez-Flores, V. M.; Murakami, N.; Ohno, T. Improvement of Photocatalytic Activity of Brookite Titanium Dioxide Nanorods by Surface Modification Using Chemical Etching. *Appl. Surf. Sci.* **2012**, *258*, 5803−5809.

(29) Fukuma, T.; Kimura, M.; Kobayashi, K.; Matsushige, K.; Yamada, H. Development of Low Noise Cantilever Deflection Sensor for Multienvironment Frequency-Modulation Atomic Force Microscopy. *Rev. Sci. Instrum.* **2005**, *76*, 053704.

(30) Fukuma, T.; Jarvis, S. P. Development of Liquid-Environment Frequency Modulation Atomic Force Microscope with Low Noise Deflection Sensor for Cantilevers of Various Dimensions. *Rev. Sci. Instrum.* **2006**, *77*, 043701.

(31) Fukuma, T. Wideband Low-Noise Optical Beam Deflection Sensor with Photothermal Excitation for Liquid-Environment Atomic Force Microscopy. *Rev. Sci. Instrum.* **2009**, *80*, 023707.

(32) Fukuma, T.; Reischl, B.; Kobayashi, N.; Spijker, P.; Canova, F. F.; Miyazawa, K.; Foster, A. S. Mechanism of Atomic Force Microscopy Imaging of Three-Dimensional Hydration Structures at a Solid-Liquid Interface. *Phys. Rev. B: Condens. Matter Mater. Phys.* **2015**, *92*, 155412.

(33) Tracey, J.; Miyazawa, K.; Spijker, P.; Miyata, K.; Reischl, B.; Canova, F. F.; Rohl, A. L.; Fukuma, T.; Foster, A. S. Understanding 2D Atomic Resolution Imaging of the Calcite Surface in Water by Frequency Modulation Atomic Force Microscopy. *Nanotechnology* **2016**, *27*, 415709.

(34) Miyata, K.; Tracey, J.; Miyazawa, K.; Haapasilta, V.; Spijker, P.; Kawagoe, Y.; Foster, A. S.; Tsukamoto, K.; Fukuma, T. Dissolution Processes at Step Edges of Calcite in Water Investigated by High-Speed Frequency Modulation Atomic Force Microscopy and Simulation. *Nano Lett.* **2017**, *17*, 4083−4089.

(35) Baur, V. W. H. Atomabstände und Bindungswinkel im Brookit, TiO₂. *Acta Crystallogr.* **1961**, *14*, 214.

(36) Rinke, P.; Qteish, A.; Neugebauer, J.; Freysoldt, C.; Scheffler, M. Combining GW Calculations With Exact-Exchange Density-Functional Theory: an Analysis of Valence-Band Photoemission for Compound Semiconductors. *New J. Phys.* **2005**, *7*, 126.

(37) Rinke, P.; Janotti, A.; Scheffler, M.; Van de Walle, C. G. Defect Formation Energies Without the Band-Gap Problem: Combining Density-Functional Theory and the GW Approach for the Silicon Self-Interstitial. *Phys. Rev. Lett.* **2009**, *102*, 026402.

(38) Beltrán, A.; Gracia, L.; Andrés, J. Density Functional Theory Study of the Brookite Surfaces and Phase Transitions Between Natural Titania Polymorphs. *J. Phys. Chem. B* **2006**, *110*, 23417−23423.

(39) Henkelman, G.; Arnaldsson, A.; Jónsson, H. A Fast and Robust Algorithm for Bader Decomposition of Charge Density. *Comput. Mater. Sci.* **2006**, *36*, 354−360.

(40) Sanville, E.; Kenny, S. D.; Smith, R.; Henkelman, G. An Improved Grid-Based Algorithm for Bader Charge Allocation. *J. Comput. Chem.* **2007**, *28*, 899−908.

(41) Tang, W.; Sanville, E.; Henkelman, G. A Grid-Based Bader Analysis Algorithm Without Lattice Bias. *J. Phys.: Condens. Matter* **2009**, *21*, 084204.

(42) Yu, M.; Trinkle, D. R. Accurate and Efficient Algorithm for Bader Charge Integration. *J. Chem. Phys.* **2011**, *134*, 064111.

(43) Varma, S.; Rempe, S. B. Coordination Numbers of Alkali Metal Ions in Aqueous Solutions. *Biophys. Chem.* **2006**, *124*, 192−199.

(44) Powell, D. H.; Neilson, G. W.; Enderby, J. E. The Structure of Cl^- in Aqueous Solution: an Experimental Determination of $g_{ClH}(r)$ and $g_{ClO}(r)$. *J. Phys.: Condens. Matter* **1993**, *5*, 5723−5730.

(45) Hiasa, T.; Kimura, K.; Onishi, H.; Ohta, M.; Watanabe, K.; Kokawa, R.; Oyabu, N.; Kobayashi, K.; Yamada, H. Solution-TiO_2 Interface Probed by Frequency-Modulation Atomic Force Microscopy. *Jpn. J. Appl. Phys.* **2009**, *48*, 08JB19.

(46) Kumar, N.; Neogi, S.; Kent, P. R. C.; Bandura, A. V.; Kubicki, J. D.; Wesolowski, D. J.; Cole, D.; Sofo, J. O. Hydrogen Bonds and Vibrations of Water on (110) Rutile. *J. Phys. Chem. C* **2009**, *113*, 13732−13740.

(47) Henderson, M. A. An HREELS and TPD Study of Water on TiO_2 (110): the Extent of Molecular versus Dissociative Adsorption. *Surf. Sci.* **1996**, *355*, 151−166.

(48) Chen, X.; Liu, L.; Yu, P. Y.; Mao, S. S. Increasing Solar Absorption for Photocatalysis with Black Hydrogenated Titanium Dioxide Nanocrystals. *Science* **2011**, *331*, 746−750.

(49) Zheng, Z.; Huang, B.; Lu, J.; Wang, Z.; Qin, X.; Zhang, X.; Dai, Y.; Whangbo, M.-H. Hydrogenated Titania: Synergy of Surface Modification and Morphology Improvement for Enhanced Photocatalytic Activity. *Chem. Commun.* **2012**, *48*, 5733−5735.